Hindawi
Advances in Condensed Matter Physics
Volume 2020, Article ID 3902835, 6 pages
https://doi.org/10.1155/2020/3902835

Research Article

Switchable Terahertz Band-Pass/Band-Stop Filter Enabled by Hybrid Vanadium Dioxide Metamaterial

Ying Chen, Jianwei Cheng, and Chaowu Liang

School of Optoelectronics, National University of Defense Technology, Changsha 410073, China

Correspondence should be addressed to Ying Chen; yinchengnudt@163.com

Received 25 August 2020; Revised 4 November 2020; Accepted 25 November 2020; Published 7 December 2020

Academic Editor: Junmin Liu

To date, little research has been carried out on the integration of switchable and diversified functionalities into a single metamaterial in the terahertz (THz) range. Here, a hybrid vanadium dioxide (VO_2) metamaterial was designed with switchable properties of band-pass filter and band-stop filter in the frequency range of 0.3–1.6 THz. Simulations demonstrated that under TE polarization, the proposed system acted as band-stop filter with the center frequency of 0.95 THz when VO_2 is in the insulating state. Upon the transformation of VO_2 into the metallic state, the proposed system behaved as a band-pass filter with a transmittance of >80%. The physical mechanism of the band-pass/band-stop conversion was examined by analyzing the surface current distribution of the designed device. The switchable characteristics of this structure can enable its wide application in tunable THz functional components such as amplitude modulators, polarization control, and intelligent switches.

1. Introduction

Metamaterials are artificial composite materials consisting of periodically arranged units that show some extraordinary electromagnetic properties including a negative refractive index [1], electromagnetically induced transparency [2], and perfect absorption [3]. Recently, metamaterial absorbers have shown great potential for application in stealth technology, detection, and communication. In 2008, Landy et al. proposed the concept of a metamaterial-based perfect absorber [3]. Due to the presence of a gap in the terahertz range, various metamaterial absorber models with different terahertz frequencies (e.g., single band [4], multiband [5, 6], and broadband absorbers [7–9]) have been proposed. However, early terahertz absorbers exhibit a single resonance mode and their absorption performance is non-tunable, limiting their potential for use in practical applications. Therefore, there is an urgent need for the development of a tunable absorber with absorption performance that can be tuned by optical, thermal, or electric excitations [10, 11].

VO_2 is an ideal thermally controlled material that undergoes a phase transition from the insulating state to the metal state at 67°C [12]. Due to this transition, transmittances of terahertz waves vary significantly before and after the phase transition so that the amplitude of terahertz waves can be controlled to a certain extent by the phase transition. Additionally, VO_2-based metamaterials that exhibit advantages such as a high modulation depth, low insertion loss, multiple driving methods, and good repeatability are currently some of the main candidates for the development of devices to achieve control of terahertz waves. Under the influence of external light and thermal excitation, a VO_2 reconfigurable metamaterial has been demonstrated to achieve various functions such as a tunable narrowband filter [13], tunable broadband absorber [14], and high-speed amplitude modulator [15]. Nevertheless, the inclusion of the additional laser and heater components may have significant effects on the integration, anti-interference ability, and production cost of such VO_2-based devices. Therefore, electric excitation is the preferred method for realizing the dynamic reconfiguration of metamaterials. Unfortunately, the electrically excited VO_2-based reconfigurable metamaterials reported to date have exhibited various limitations and disadvantages. For example, in 2011, Jeong et al. reported an electrically excited VO_2 reconfigurable

metamaterial. However, the voltage required for reconfiguration was as high as 500 V [16]. In subsequent work based on this approach, Liu et al. designed a multilayer composite structure to achieve high-speed modulation for mid-infrared signals with a trigger time of only 0.25 s. However, the current required for the operation of this device was as high as 4 A [17]. In 2017, Zhou et al. shaped VO_2 into a grid form that was then inserted in the middle of the metal comb, obtaining the modulation depth of 87% in a wide frequency range of 0.4–1.2 THz and reducing the required current to 0.5 A. However, this device must be preheated to approximately 68°C for operation [18]. Recently, Park et al. fabricated a narrow-band filter in the terahertz frequency band by ingeniously designing the upper metal structure of a VO_2-reconfigurable metamaterial and using the strong coupling characteristics of metal structure so that a driving voltage of only 5.5 V was required. However, the fabricated device showed a high insertion loss, and the maximum transmission rate was only 43% [19].

In summary, investigations of the electrically excited VO_2 metamaterials have attracted intense attention in the research and development of terahertz functional devices. Due to the need to ensure a low insertion loss, the current research effort has focused on enabling more flexible functions, higher modulation depth, faster response rate, and lower driving power of these devices. In the development of terahertz filters, Chen et al. proposed an adjustable terahertz absorber with a multidefect combination-embedded VO_2 film structure that can control the phase change of VO_2 by changing the external environment temperature and enable the variation of the absorption rate at two frequencies from 99.8% to 1.0% [20]. Ma et al. introduced the conceptual design of the fractal Koch curve and fabricated a novel terahertz band-pass filter. They showed that the resonant frequency of the filter was 0.715 THz, the transmission coefficient reached 0.92, and the −3 dB bandwidth was 21.9 GHz [21]. Li et al. proposed a switchable dual-control terahertz broadband absorber based on a hybrid graphene-VO_2 metamaterial. Numerical simulations showed that the amplitude of the broadband absorption band (1.69–3.21 THz) can be dynamically adjusted from 25.4% to 99.2% by adjusting the electronic conductivity of VO_2 [22]. Zhang et al. proposed a vanadium dioxide-based multilayer metamaterial with bifunctional properties of absorption and polarization conversion. It was found that the designed system behaves as a single-band absorber when vanadium dioxide is in the metallic state and behaves as a cross-polarization converter when vanadium dioxide is in the insulating state [23]. Chen et al. achieved the dual functionalities of perfect absorption and high transmission in a single metamaterial by introducing vanadium dioxide film into a multilayer structure. Their device acts as a narrowband absorber when vanadium dioxide is in the conducting state and acts as a transparent conducting metal when vanadium dioxide is in the insulating state [24, 25].

In this work, a metamaterial filter with a metal structure unit composed of two horizontally placed riveted metal oscillators and a vertical metal strip was designed and examined by electromagnetic simulations. The rectangular VO_2 film is located underneath the metal structure. Simulation results show that in the TE mode, when VO_2 was in the insulating state, this device exhibits the characteristics of a band-stop filter with the band-stop central frequency of 0.95 THz. When VO_2 changed to the metal state, the band-stop characteristics of the device disappeared gradually and transmission at the central frequency increased from 1% to 80%, while transmission in other frequency bands gradually decreased and the device exhibited band-pass characteristics.

2. Design of Device Structure

In this work, a type of commercial full wave CST 2019 microwave studio simulation software (3DS, USA) is used to model the device. Figure 1(a) schematically illustrates the three-dimensional unit structure of the proposed terahertz filter, while Figure 1(b) shows the side view of the unit structure. Here, the electric field of the terahertz wave is along the x-direction (TE mode), the magnetic field of the terahertz wave is along the y-direction, and the incident direction of terahertz wave is normal incidence.

The entire device is a multilayer structure, and the side view of its unit structure is shown in Figure 1(b). From bottom to top, the device consists of a silicon substrate (dielectric constant $\varepsilon = 11.9$), silicon nitride ($\varepsilon = 7$, loss tangent = 0.05), and a metal layer (aluminum, electronic conductivity $\sigma = 3.56 \times 107$ S/m) with a rectangular VO_2 film embedded in the center of the silicon nitride layer. Figure 1 shows the top view of the metal structure and the VO_2 film. The metal unit structure is composed of two horizontal riveted metal oscillators and a vertical metal strip, and the rectangular VO_2 layer is located directly below the metal structure, where L_1 and L_2 are the unit side lengths, W is the line width of all metals, L is the width of VO_2 (the VO_2 length is L_2), and s denotes the interval between the riveted oscillator and the metal strip. All of the units are arranged periodically, and the upper side is connected to the positive electrode, while the lower side is connected to the negative electrode, so that the device structure is formed as shown in Figure 1. The filter dimensions are approximately 1 cm × 1 cm, and the width of left and right electrodes is approximately 60 μm. The thickness of the silicon layer used in the simulation is 35 μm, the thickness of the silicon nitride layer is 500 nm, and the thickness of the VO_2 layer in the middle is 120 nm. The final optimized structure parameters are set to $L_1 = L_2 = 85$ μm, $s = 7$ μm, $L = 55$ μm, and $W = 5$ μm.

3. Simulation of the Device Performance

The simulation of the device used a frequency-domain solver that was set to the unit cell bound in both the x- and y-directions, and in the z-direction, the boundary condition of incident surface was set to open addspace, while the boundary condition of the detection surface was set to open to avoid the occurrence of Fabry–Pérot oscillation. In the simulation, we simulated the electric excitation of the device by changing the electronic conductivity of VO_2.

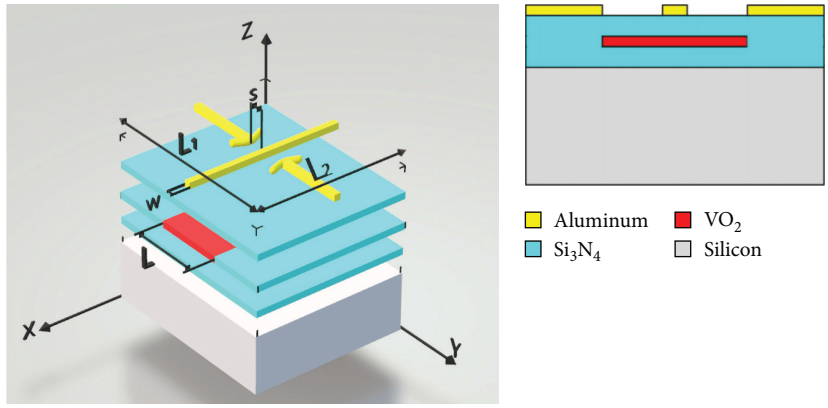

(a) (b)

Figure 1: (a) Three-dimensional schematic diagram of the unit structure of the device. (b) Side view of the unit structure. White: silicon; blue: silicon nitride; red: VO_2; yellow: aluminum.

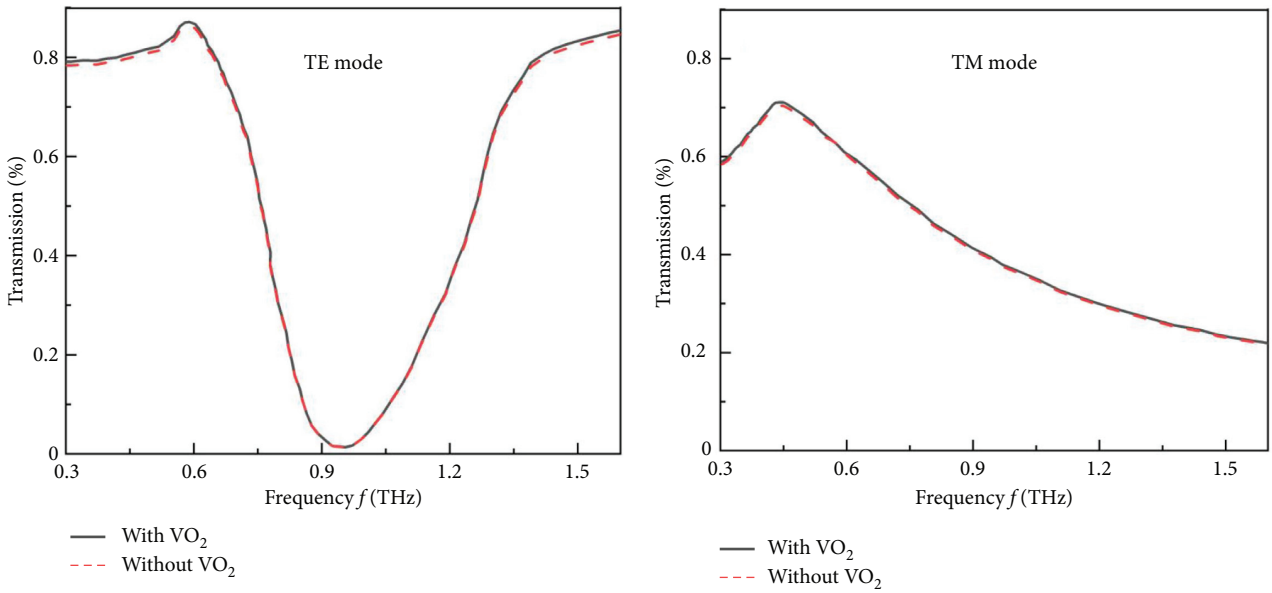

(a) (b)

Figure 2: Influence of VO_2 on the transmission spectrum of the device under (a) TE mode and (b) TM mode.

First, our numerical simulations studied the effect of the insertion of the VO_2 film in the insulating state (with electronic conductivity of 0.5 Ω^{-1} cm^{-1}) on the transmission spectrum of this device. The results of the simulations are shown in Figure 2 and suggest that the inserted VO_2 film has little effect on the transmission spectrum in the range of 0.3–1.6 THz for both TE and TM modes.

Then, we changed the electronic conductivity of VO_2 to simulate the dynamic changes of its transmission spectrum when the device is electrically excited. Figure 3(a) shows the evolution of the transmission spectrum when VO_2 changed from the insulating state to the metal state with the electronic conductivity of 30,000 Ω^{-1} cm^{-1}. It is observed that under the TE mode, the transmission at the central frequency of 0.95 THz gradually increased with increasing electronic conductivity of VO_2. For the electronic conductivity of VO_2 of 30,000 Ω^{-1} cm^{-1}, the transmission at 0.95 THz increased from 1% to approximately 81%. This implies that at this frequency, the device gradually changes from the band-stop filter to the band-pass filter. Meanwhile, the behavior of the material for the frequency bands on the left (such as 0.5 THz) and right (such as 1.4 THz) sides of central frequency changed from band-pass to band-stop filter, and transmission was reduced from 80% to 8%. Thus, under electric field excitations, the proposed filter achieved transition from band-pass to band-stop filter in the frequency range of 0.3–1.6 THz due to phase transition of the VO_2 layer. Additionally, the central frequencies of the band-pass and band-stop filter are almost the same.

Figure 3(b) describes the influence of the electronic conductivity of VO_2 on the transmission spectrum of device under the TM mode. It is observed that when VO_2 was in the

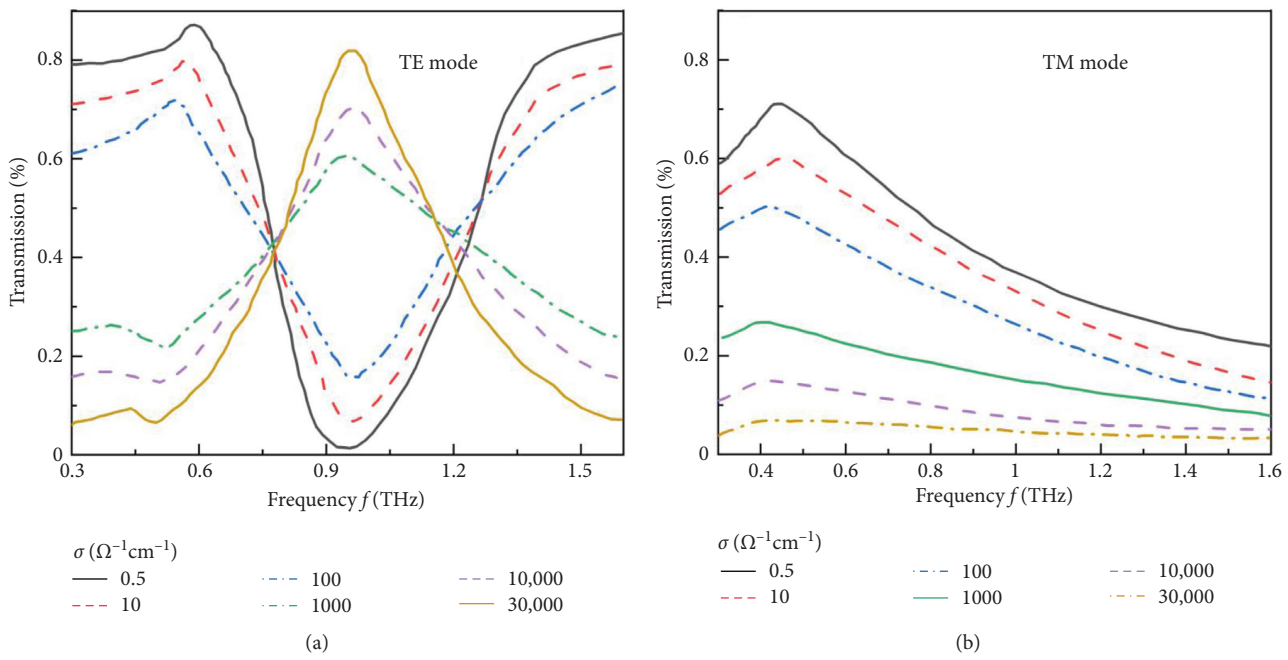

Figure 3: Transmission spectra of the device for different electronic conductivities under (a) TE mode and (b) TM mode.

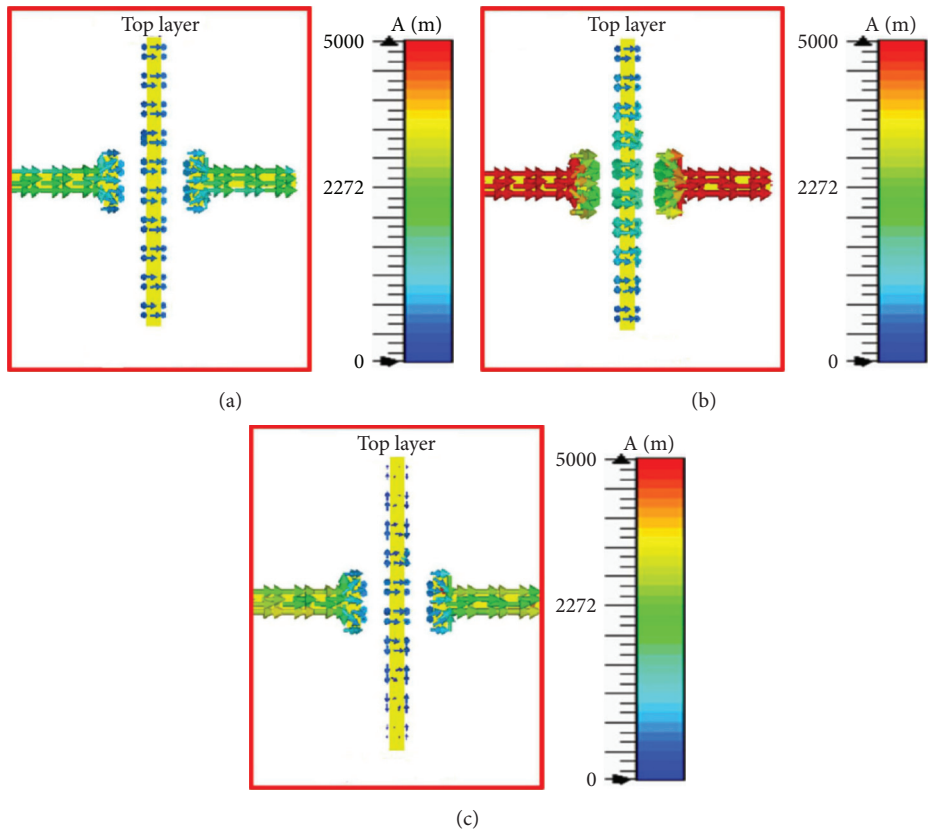

Figure 4: Surface current distribution for the device when VO_2 is in the insulating state for the frequencies of (a) 0.6 THz, (b) 0.95 THz, and (c) 1.4 THz.

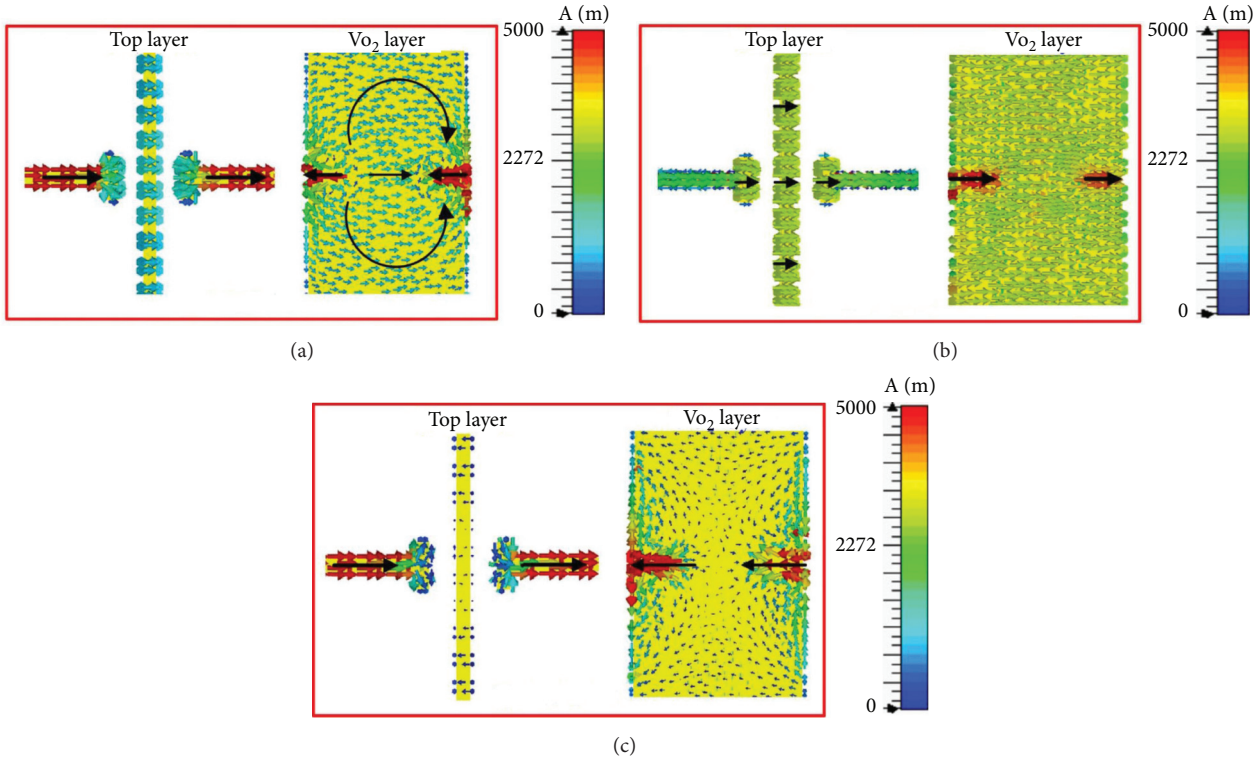

Figure 5: Surface current distribution of the device when VO_2 is in the metal state for the frequencies of (a) 0.6 THz, (b) 0.95 THz, and (c) 1.4 THz.

insulating state, the transmission of the device was higher than 50% in the range of 0.3–0.8 THz. As VO_2 gradually changed to the metal state, its transmission decreased in a wide frequency range and eventually was lower than 5%. Thus, due to the lack of symmetry of the unit structure, the proposed device exhibited completely different characteristics under TE and TM modes.

4. Physical Mechanism of Band-Pass to Band-Stop Transition of the Device

To investigate the physical mechanism of the conversion from a band-pass filter to a band-stop filter under the TE mode, the surface currents in the device before and after the VO_2 phase transition were simulated. When VO_2 was in the insulating state, the device exhibited band-stop characteristics and its surface current is shown in Figure 4. For the terahertz wave frequencies of 0.6 THz and 1.4 THz, the surface current in the device was mainly concentrated on the riveting-type oscillator and was approximately 2300 A/m. For the terahertz wave frequency of 0.95 THz, the current reached 4800 A/m, demonstrating that the band-stop behavior in this device at 0.95 THz is caused by the strong surface current on the riveted oscillator and that the transmission in the left and right frequency bands is higher because the oscillation current is small and its influence on the transmittance is low, giving rise to the band-pass characteristics.

When VO_2 was in the metal state, the device displayed band-pass behavior and its surface current is shown in Figure 5. Obviously, a strong surface current was observed only when VO_2 was in the metal state. In Figure 5, the VO_2 layer in the metal state is marked in yellow. As shown in Figure 5(a), both the top riveted oscillator and the VO_2 layer underneath the oscillator produced surface currents at the incident terahertz wave frequency of 0.6 THz. Meanwhile, the direction of the strong current oscillation on the sides of VO_2 was opposite to that of the metal structure. Therefore, the oscillation effects of these two strong currents canceled each other out. It can be concluded that the band-stop characteristics in the low-frequency region are mainly caused by the weak current that oscillates on the VO_2 surface. Figure 5(b) shows the surface currents on the metal layer and the VO_2 layer with for the incident terahertz wave frequency of 1.4 THz. In this case, the current was mainly concentrated on both sides of the VO_2 layer for dipole oscillation and its dipole moment was small, giving rise to the band-stop characteristics in the high-frequency region of the spectrum. Figure 5(c) shows the surface currents on the metal layer and the VO_2 layer for the incident terahertz wave frequency of 0.95 THz. It is observed that strong oscillation currents on these two layers propagated in opposite directions and canceled each other out. In this case, the surface current on VO_2 was extremely weak. Therefore, the device showed band-pass characteristics at 0.95 THz.

5. Conclusions

A VO_2-based terahertz filter has been proposed in this work, and numerical simulations revealed that the proposed device

can achieve conversion from band-stop to band-pass filter under the TE mode. When VO_2 is in the insulating state (electronic conductivity = 0.5 Ω^{-1} cm^{-1}), the device exhibited the characteristics of a band-stop filter with the central frequency of 0.95 THz. When VO_2 transitioned to the metal state (electronic conductivity = 30,000 Ω^{-1} cm^{-1}), the transmission of the device at the central frequency increased from 1% to 80%, while its transmission at the other frequency bands decreased and the device transformed from the band-stop to the band-pass filter. Under the TM mode, the proposed device displayed the characteristics of a broadband terahertz amplitude modulator. Due to the phase transition of VO_2, the spectrum transmission varied between 50% and 5% in the frequency range of 0.3–0.8 THz. Because of its simple structure, facile fabrication, function tunability, and low cost, the proposed filter is highly promising for use in future terahertz systems.

Data Availability

The simulation and figure data used to support the findings of this study are all included within the article.

Conflicts of Interest

The authors declare that they have no conflicts of interest.

Acknowledgments

This work was supported by the National Natural Science Foundation of China, under Grant no. 61808016.

References

[1] R. A. Shelby, D. R. Smith, and S. Schultz, "Experimental verification of a negative index of refraction," *Science*, vol. 292, no. 4, pp. 77–79, 2001.

[2] S. Zhang, D. A. Genov, Y. Wang et al., "Plasmon-induced transparency in metamaterials," *Physical Review Letters*, vol. 101, no. 4, pp. 218–221, 2008.

[3] N. I. Landy, S. Sajuyigbe, J. J. Mock, D. R. Smith, and W. J. Padilla, "Perfect metamaterial absorber," *Physical Review Letters*, vol. 100, no. 20, pp. 1–4, 2008.

[4] Y. B. Long, L. Shen, H. T. Xu et al., "Achieving ultranarrow graphene perfect absorbers by exciting guided-mode resonance of one-dimensional photonic crystals," *Scientific Reports*, vol. 6, Article ID 32312, 2016.

[5] Q. Y. Wen, H. W. Zhang, Y. S. Xie et al., "Dual band terahertz metamaterial absorber: design, fabrication, and characterization," *Applied Physics Letters*, vol. 95, no. 24, Article ID 241111, 2009.

[6] Z. Y. Bao, J. C. Wang, Z. D. Hu et al., "Coordinated multiband angle insensitive selection absorber based on graphene metamaterials," *Optics Express*, vol. 27, no. 22, Article ID 31435, 2019.

[7] M. Chen, F. Fan, L. Yang et al., "Broadband terahertz metamaterial absorber based on double composite structure layer," *Chinese Journal of Lasers*, vol. 46, no. 6, Article ID 0614034, 2019.

[8] Y. B. Zhang, W. W. Liu, L. C. Li et al., "Ultrathin polarization-insensitive wide-angle broadband near-perfect absorber in the visible regime based on few-layer MoS_2 films," *Applied Physics Letters*, vol. 111, no. 11, Article ID 111109, 2017.

[9] S. Q. Chen, H. Cheng, H. F. Yang et al., "Polarization insensitive and omnidirectional broadband near perfect planar metamaterial absorber in the near infrared regime," *Applied Physics Letters*, vol. 99, no. 25, Article ID 253104, 2011.

[10] J. Bai, S. Zhang, F. Fan et al., "Tunable broadband THz absorber using vanadium dioxide metamaterials," *Optics Communications*, vol. 452, pp. 292–295, 2019.

[11] Y. T. Zhao, B. Wu, B. J. Huang, and Q. Cheng, "Switchable broadband terahertz absorber/reflector enabled by hybrid graphene-gold metasurface," *Optics Express*, vol. 25, no. 7, p. 7161, 2017.

[12] N. Mott, "On metal-insulator transitions," *Journal of Solid State Chemistry*, vol. 88, no. 1, pp. 5–7, 1990.

[13] V. Sanphuang, N. Ghalichechian, N. K. Nahar, and J. L. Volakis, "Reconfigurable THz filters using phase-change material and integrated heater," *IEEE Transactions on Terahertz Science and Technology*, vol. 6, no. 4, pp. 583–591, 2016.

[14] F. Ding, S. Zhong, and S. I. Bozhevolnyi, "Vanadium dioxide integrated metasurfaces with switchable functionalities at Terahertz Frequencies," *Advanced Optical Materials*, vol. 6, no. 9, Article ID 1701204, 2018.

[15] Y. Zhang, S. Qiao, L. Sun et al., "Photoinduced active terahertz metamaterials with nanostructured vanadium dioxide film deposited by sol-gel method," *Optics Express*, vol. 22, no. 9, pp. 11070–11078, 2014.

[16] Y. G. Jeong, H. Bernien, J. S. Kyoung et al., "Electrical control of terahertz nano antennas on VO_2 thin film," *Optics Express*, vol. 22, no. 19, pp. 21211–21215, 2011.

[17] L. Liu, L. Kang, T. S. Mayer et al., "Hybrid metamaterials for electrically triggered multifunctional control," *Nature Communications*, vol. 7, Article ID 13236, 2016.

[18] G. Zhou, P. Dai, J. Wu et al., "Broadband and high modulation-depth THz modulator using low bias controlled VO_2-integrated metasurface," *Optics Express*, vol. 25, no. 15, pp. 17322–17328, 2017.

[19] D. J. Park, J. H. Shin, K. H. Park, and H. C. Ryu, "Electrically controllable THz asymmetric split-loop resonator with an outer square loop based on VO_2," *Optics Express*, vol. 26, no. 13, pp. 17397–17406, 2018.

[20] X. S. Chen and J. S. Li, "Tunable terahertz absorber with multi-defect combination embedded VO_2 thin film structure," *Acta Physica Sinica*, vol. 69, no. 2, Article ID 027801, 2020.

[21] H. Y. Ma and J. S. Li, "Terahertz bandpass filter based on Koch curve fractal structure," *Spectroscopy and Spectral Analysis*, vol. 40, no. 3, pp. 733–737, 2020.

[22] H. Li, J. Yu, and Z. Chen, "Broadband tunable terahertz absorber based on hybrid graphene-vanadium dioxide metamaterial," *Chinese Journal of Lasers*, vol. 47, no. 9, Article ID 0903001, 2020.

[23] M. Zhang, J. Zhang, A. Chen, and Z. Song, "Vanadium dioxide-based bifunctional metamaterial for terahertz waves," *IEEE Photonics Journal*, vol. 12, no. 1, pp. 1–9, 2020.

[24] L. Chen and Z. Song, "Simultaneous realizations of absorber and transparent conducting metal in a single metamaterial," *Optics Express*, vol. 28, no. 5, pp. 6565–6571, 2020.

[25] J. H. Shin, S. P. Han, M. Song, and H. C. Ryu, "Gradual tuning of the terahertz passband using a square-loop metamaterial based on a W-doped VO_2 thin film," *Applied Physics Express*, vol. 12, no. 3, Article ID 032007, 2019.